The Astrophysical Journal, 620:523–536, 2005 February 10

UVCS OBSERVATION OF SUNGRAZER C/2001 C2: POSSIBLE COMET FRAGMENTATION AND PLASMA-DUST INTERACTIONS

A. Bemporad,[1] G. Poletto,[2] J. C. Raymond,[3] D. A. Biesecker,[4] B. Marsden,[3]
P. Lamy,[5] Y.-K. Ko,[3] and M. Uzzo[3]

Received 2004 June 14; accepted 2004 October 21

ABSTRACT

In this paper we analyze *SOHO* Ultraviolet Coronagraph Spectrometer (UVCS) observations of the sungrazing comet C/2001 C2, a member of the Kreutz family, observed on 2001 February 7 at heliocentric distances of 4.98 and 3.60 $R_\odot$. This comet apparently went through sequential fragmentation events along its path: further indication of fragmentation processes is provided by UVCS observations, which show the presence of two separate tails in the 4.98 $R_\odot$ data set, which we interpret as two fragments unresolved by LASCO images, one of which sublimates before reaching 3.60 $R_\odot$. The cometary hydrogen Lyα signal, decaying exponentially with time, has been interpreted in terms of the H_2O outgassing rate and the interactions of coronal protons with atoms created by the photodissociation of water. However, one of the fragments shows an additional Lyα contribution, constant with time, which adds to the temporally decaying signal. This contribution has been ascribed to the sublimation of pyroxene dust grains, whose end products neutralize coronal protons via charge exchange processes. Hence, the two fragments have different composition; differences throughout the comet body may have been the primary cause for the comet fragmentation.

Subject headings: comets: general — comets: individual (C/2001 C2) — ultraviolet: general

1. INTRODUCTION

The first definitely recognized member of what came to be known as the Kreutz sungrazing comet group was C/1843 D1. Shortly after that comet appeared, Cooper (1843) noted its similarity to comets C/1668 E1 and X/1702 D1, the possible mutual identity of which had already been remarked on by J. D. Cassini (Bion 1751, p. 97). A new reduction by Henderson (1843) of some 1668 observations seemed to confirm the 1668-1843 linkage but rendered a connection to the 1702 comet unlikely. Although observations of four further sungrazing comets between 1880 and 1887 gave rise to another round of speculations that just a single short-period comet was involved, Kirkwood (1880) had already entertained the possibility that comets C/1843 D1 and C/1880 C1 were a discrete pair. This paved the way for Kreutz (1888) to begin his detailed study of a cometary complex that probably included the aforementioned comets and possibly also comet X/1106 C1.

After further sungrazing comets had been observed in the midtwentieth century, it seemed evident that there were two distinct Kreutz subgroups, and Marsden (1967) demonstrated unequivocally that the two best observed members of one subgroup, C/1882 R1 and C/1965 S1, must have broken off from each other around the time of their previous perihelion passage (much as these comets were individually seen to split), perhaps then having been recorded as the 1106 comet. Later Marsden (1989) presented a possible scenario for a similar separation of C/1963 R1 from the presumed parent of the 1843 and 1880 members. During 1979–1989, with the discovery of 16 presumed members from space by the SOLWIND instrument on the *P78-1* satellite and the coronagraph aboard the *Solar Maximum Mission*, it became apparent that the Kreutz comets were substantially more numerous than had been thought. Since 1996, the two LASCO cameras (see below) aboard the *SOHO* mission have detected almost 700 of these objects (as well as more than 100 non-Kreutz comets),[6] with sometimes two or three approaching the Sun on the same day. Although the orbits computed for these comets should not be considered precise orbit determinations, there are often obvious differences between the orbit planes of members appearing only hours apart, a circumstance that requires many of the separations to have taken place when the comets were far from the Sun (Sekanina 2002). Very recently, Sekanina & Chodas (2004) have published an intriguing scenario involving splitting both close to and far from the Sun that is thereby able to relate members of the different Kreutz subgroups.

Many studies have been performed on the variation of sungrazer magnitude with the heliocentric distance of observation (namely, the cometary light curves) aimed at modeling the observed shape and the heliocentric distance at which the visual magnitude peaks. Because of the increase in solar flux, the typical sungrazer light curve shows a rapid increase in intensity as the comet approaches the Sun; because the V magnitude is dominated by light scattered by dust, this increase corresponds to an increase in the total cross-sectional area of dust particles exposed to the solar flux, related in part to an increase in the rate of gas and dust production. Then, after a peak in intensity, the light curve rapidly decreases, probably because coma dust grains sublimate at a rate that exceeds the production rate.

The large number of observations have made it possible to perform some statistical investigation of the comet orbits and to obtain more information about the possible progenitor comet. In particular, Biesecker et al. (2002) studied the light curves of the 141 Kreutz family sungrazers observed with LASCO from

[1] Dipartimento di Astronomia e Scienza dello Spazio, Università di Firenze, Largo Enrico Fermi 5, 50125 Florence, Italy; bemporad@arcetri.astro.it.
[2] INAF-Osservatorio Astrofisico di Arcetri, Largo Enrico Fermi 5, 50125 Florence, Italy; poletto@arcetri.astro.it.
[3] Harvard-Smithsonian Center for Astrophysics, 60 Garden Street, Cambridge, MA 02138; jraymond@cfa.harvard.edu.
[4] Space Environment Center R/SE, 325 Broadway, Boulder, CO 80305.
[5] Laboratoire d'Astronomie Spatiale, CNRS, BP8, 13376 Marseille Cedex 12, France.

[6] See http://ares.nrl.navy.mil/sungrazer.

1996 through 1998 and identified two different typical light curves (independent of coma brightness) with the main peaks at 11.2 and 12.3 $R_\odot$, possibly depending on differences in the properties of the cometary dust. In every case, however, the fading after the main peak stops at about 7 $R_\odot$ and is followed by inconsistencies between different light curves: in some cases the light curve flattens, while in other cases there are some secondary increases in brightness. Biesecker et al. anticipated that a disruption of the nucleus due to thermal or gravitational stresses or both can cause this behavior.

Subsequent works interpreted the light-curve shape as a consequence of two different phenomena: sublimation of fluffy aggregates of crystalline olivine ($[Mg, Fe]_2SiO_4$) and pyroxene ($[Mg, Fe]_2Si_2O_6$) grains (Kimura et al. 2002) and/or erosion and fragmentation events of the cometary nucleus (Sekanina 2003). In particular, Kimura et al. (2002) observed that in sungrazing comets the primary dust constituent materials are probably silicates, and they modeled the dust sublimation, finding that "each observed lightcurve is a superposition of two distinct lightcurves originating from olivine and pyroxene grains." The authors showed that the two different main peak positions observed in light curves of different sungrazers at 11.2 and 12.3 $R_\odot$ are a consequence, respectively, of crystalline and amorphous olivine dust grain sublimation. Moreover, the brightness features below 7 $R_\odot$ have been explained by Sekanina (2003) by introducting an erosion model for the *SOHO* sungrazers, leading to the conclusion that "there is nothing inconsistent about them if one allows the existence of subfragments with a lower than average susceptibility to erosion." The subfragments, given the large pixel size of the coronagraph detectors, are in general optically unresolved; however, the author showed that, by introducing one or more nearby companions with a slower erosion rate, it is possible to reproduce the observed light curves of many sungrazers.

Over the last few years, two sungrazing comets have been observed in the Lyα line by the Ultraviolet Coronagraph Spectrometer (UVCS) on board *SOHO* (Raymond et al. 1998; Uzzo et al. 2001); from these observations the authors derived outgassing rates, the sizes of the nuclei, and coronal parameters including electron density, kinetic temperature, and solar wind speed. In particular, Uzzo et al. (2001) inferred from Lyα observations of the C/2000 C6 sungrazer the presence of a slowly eroding subfragment not resolved by the white-light coronagraphs.

In this work, we focus on the sungrazing comet C/2001 C2 (SOHO-294 in the *SOHO* team's numbering), a member of the Kreutz family observed on 2001 February 7 by UVCS and LASCO between the projected distances (on the plane of the sky) of 7.41 and 1.78 $R_\odot$. This comet is similar to the sungrazer C/2000 C6 studied by Uzzo et al. (2001) but shows evidence for a long-lasting Lyα component that we attribute to dust. In § 2 we give a description of the UVCS and LASCO data; in § 3 we discuss the physics of cometary line formation (§ 3.1) and the origin of a secondary component observed in the Lyα line profile (§ 3.2). In § 4 we give a summary of the model used to interpret the observed Lyα emission, showing that a contribution from pyroxene dust grains is essential to reproduce the long-lasting Lyα component observed at 4.98 $R_\odot$. A short summary of our results concludes the paper.

2. OBSERVATIONS

2.1. *LASCO Data*

The two LASCO C2 and C3 experiments aboard the *SOHO* spacecraft are externally occulted coronagraphs observing the white-light solar corona with fields of view that observe, respectively, from 2.0 to 6.0 $R_\odot$ and from 3.7 to 30.0 $R_\odot$. The "synoptic" observations are made with C2 using an orange filter ($\lambda \sim 540$–640 nm), while C3 observes with a clear filter ($\lambda \sim 400$–850 nm); for a more complete instrumental description, see Brueckner et al. (1995). Typical LASCO data consist of a sequence of images taken at the rate of about 1 every 24 minutes, typically viewed as "movies."

In Figure 1 we show the visual appearance of the comet C/2001 C2 as seen by the LASCO C3 coronagraph on 2001 February 7. The comet approached the Sun from the southeast quadrant at a position angle (i.e., the angle measured counterclockwise from celestial north through east) of about 100°, projected onto the plane of the sky. Superposed on the LASCO images, we show also the orbit of the comet, computed from the orbital parameters given in the Minor Planet Electronic Circular (MPEC) 2001-C09 and projected onto the plane of the sky. Table 1 gives, at each projected heliocentric distance of the UVCS slit $R_{\rm sky}$, the computed cometary heliocentric distance r, the times $t_{\rm ent}$ at which the comet first enters the UVCS slit, the Earth-comet distance δ, the cometary velocity v, the radial component v_r, the component $v_{\rm LOS}$ along the line of sight, and the component $v_{\rm slit}$ along the UVCS slit (i.e., the component along the UVCS slit of the cometary velocity projected onto the plane of the sky). The low $v_{\rm slit}$-values in this table with respect to the cometary velocity v indicate that the UVCS slit was roughly perpendicular to the comet trajectory, as also shown in Figure 1.

From LASCO observations, comet C/2001 C2 showed a maximum tail length of 0.°2 and was the second bright comet in 2 days: it followed nearly the same path as the comet C/2001 C3 (observed on 2001 February 6), possibly indicating that a fragmentation event occurred farther from the Sun, before our observations (see below). As C/2001 C2 approached the Sun, it progressively disappeared from the LASCO images and completely sublimated before perihelion.

The observation of one or two fragments in the C/2001 C2 LASCO white-light images has been extensively discussed: in the LASCO Comets Report,[7] the identification of subfragments is claimed by the LASCO team, and two images of the subfragments were reported by M. Oates.[8] However, there is no conclusive evidence in the white-light images for the identification of such fragments, because no background-corrected images have been made available by the LASCO team. Nevertheless, we note that the lack of resolvable fragments does not contradict the identification, later on in this work, of two fragments in the UVCS data: as we anticipate in § 1, the introduction of one or more fragments unresolved in the LASCO images allowed Sekanina (2003) to reproduce the observed light curves of many sungrazers, keeping in mind that "no multiplicity would be discerned even if a breakup had occurred as early as ~40 days before perihelion" (Sekanina 2003). Moreover, from UVCS observations of sungrazer C/2000 C6, Uzzo et al. (2001) inferred the presence of a subfragment, and this was not resolved in the white-light images, either. Because in our case the spatial resolution of the UVCS observations is higher than the resolution of the LASCO coronagraph (see § 2.2), we are able to resolve objects that are unresolved in the LASCO data.

Figure 2 gives the C/2001 C2 light curve built from observations acquired by the LASCO C2 and C3 coronagraphs. This plot shows the apparent magnitudes: normalization to

[7] See http://ares.nrl.navy.mil/sungrazer/comets_found.old/comets_2001/comets200102_arch.html.

[8] See http://www.ph.u-net.com/comets/20010207_fragments.gif.

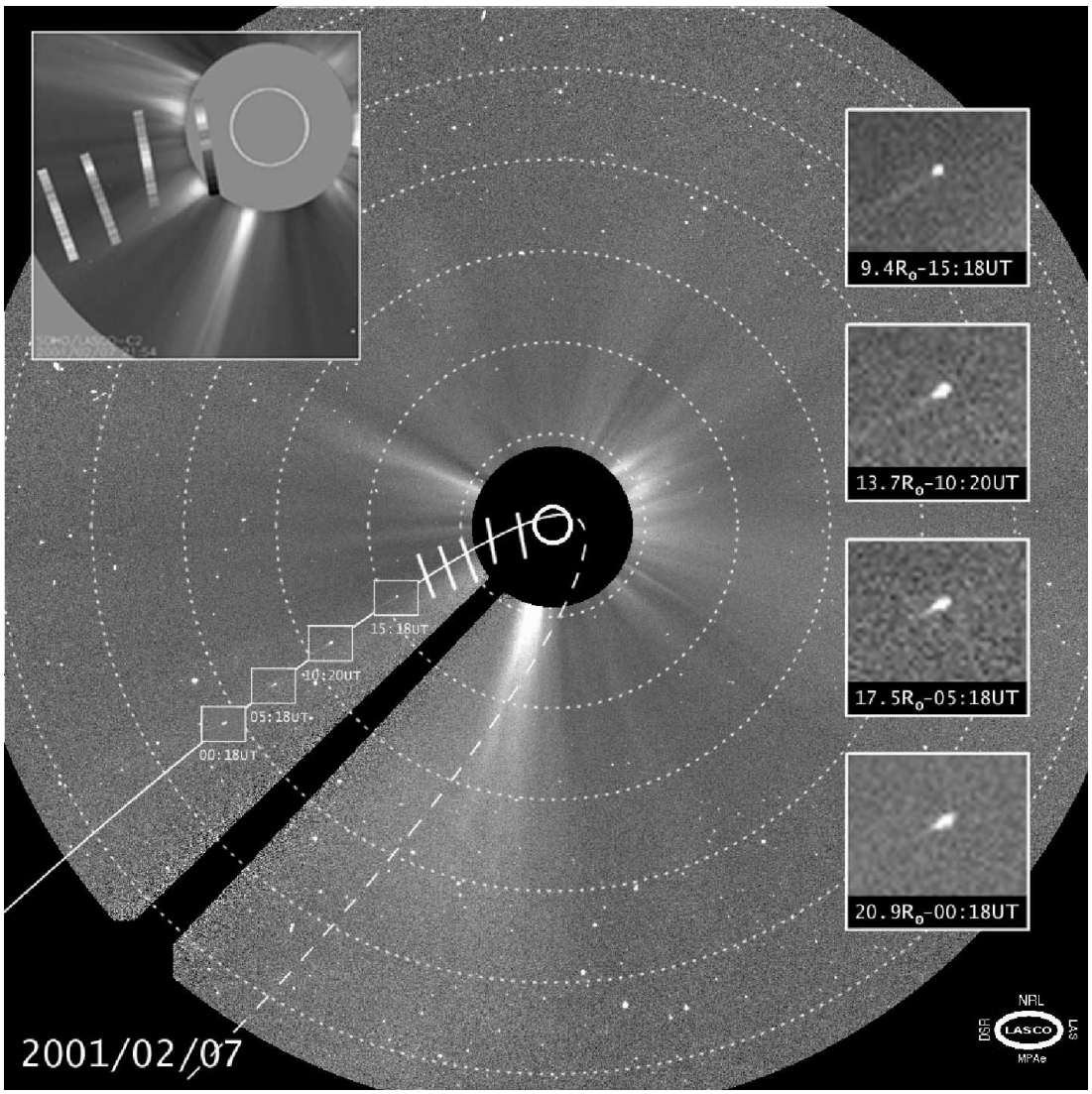

FIG. 1.—C/2001 C2 as observed by LASCO C3. We superposed onto the 2001 February 7, 10:42 UT LASCO C3 frame the cometary LASCO C3 images at 00:18, 05:18, 10:20, and 15:18 UT (*right insets*); the different UVCS slit heliocentric distances are also shown. The dotted circles are drawn at 5, 10, 15, 20, 25, and 30 $R_\odot$. To compare the orbit of the comet with the positions of the UVCS slit, we plotted also the preperihelion (*solid line*) and expected postperihelion (*dashed line*) C/ 2001 C2 trajectory as computed from the orbital parameters. To show the coronal morphology at lower levels, we superpose onto the LASCO C2, 21:54 UT image (*left inset*) the UVCS Lyα coronal intensity before the comet arrival at the projected heliocentric distances of 1.78, 3.44, 4.94 and 6.17 $R_\odot$ (the UVCS Lyα at 7.41 $R_\odot$ has not been plotted because it is out of the LASCO C2 field of view).

1 AU would reduce the brightness by 0.15 mag at the edge of the LASCO C3 field. The correction decreases as the comet approaches the Sun, reaching 0.06 mag in the region where the UVCS observations were obtained. These corrections are within the uncertainties of the magnitude measurements, so they are not included in Figure 2. In this figure we note that, after the main peak of the light curve at $\sim$12.1 $R_\odot$, C/2001 C2 brightens again, starting from $\sim$5.3 $R_\odot$. There are two plausible explanations: one possibility is that the comet fragments at about 5.3 $R_\odot$, exposing more surface area to sunlight and increasing its outgassing rate for a short time until the fragments sublimate. The other possibility, following Sekanina (2003), is that a fragmentation of the cometary nucleus occurred farther from the Sun: if the fragment traveling with the comet has a lower erosion rate than the main nucleus, it can survive after the disintegration of the main part and can be observed in the white light below $\sim$5.3 $R_\odot$ (Fig. 2, *gray zone*). This implies that the fragment material had on average a higher heat of sublimation than the material of the main comet: the fragment was a rocky part of the main comet that contained a higher percentage of minerals. As we show in § 4.2, the latter scenario agrees with the presence of pyroxene dust grains inferred by UVCS data in one of the two objects that we observed.

The fragmentation of the C/2001 C2 nucleus has been studied also by Sekanina (2002): the author compared the orbital parameters of this comet with those of other sungrazers, finding evidence from sungrazer pairs for runaway fragmentation events that occurred at large heliocentric distances, before the comets were detected. In particular, the author, analyzing the comet's relative motions, concluded that the C/2001 C2 comet may have been involved in up to three fragmentation events before being observed by *SOHO*. The orbital parameters of these three comets (C/2001 B3, C/2000 B5, and C/1999 V2) are given in Table 2: we note that all parameters (with the obvious exception of their perihelion times $T_{\rm peri}$) are very similar to those of the C/2001 C2 comet and different, for instance, from the orbital parameters of another Kreutz sungrazer (C/2001 C4) seen just after our comet. Moreover, as we said above, 1 day

TABLE 1
C/2001 C2 Observational and Kinematic Parameters

R_{sky} ($R_\odot$)	r ($R_\odot$)	t_{ent} (UT)	δ (AU)	v (km s^{-1})	v_r (km s^{-1})	v_{LOS} (km s^{-1})	v_{slit} (km s^{-1})
7.41.....	7.416	...	0.9988	226.7	210.0	84.25	55.42
6.17.....	6.172	...	1.001	248.5	226.3	84.11	57.79
4.94.....	4.981	19:19:10	1.003	276.6	245.7	81.40	58.18
3.44.....	3.600	20:19:15	1.005	325.4	273.7	69.28	107.6
1.78.....	2.204	...	1.006	415.9	300.5	17.53	112.8

Note.—For t_{ent}-values, see t_{st} in Table 4.

before our observations, on 2001 February 6, LASCO observed another Kreutz sungrazer (C/2001 C3) following about the same trajectory as C/2001 C2, with orbital parameters similar to those of our comet (see Table 2).

The collected evidence suggests that the material of the C/2001 C2 nucleus tended to break up very easily, making it likely to observe those fragments as the comet approached the Sun in the final phase of its life. In § 2.2 we discuss the possible origins for the two tails we observed in the 4.98 $R_\odot$ UVCS data and the cometary disintegration below 3.60 $R_\odot$.

2.2. *UVCS Data*

The UVCS aboard the *SOHO* satellite consists of two channels for the observation of spectral lines in the UV range (namely, the O VI and Lyα channels) and one white-light channel. In this work, we analyze data acquired by the O VI channel, which is optimized for observations in the spectral range around the O VI $\lambda\lambda$1031.90, 1037.63 doublet and, at the selected grating position, covers the interval from 984 to 1080 Å in the first order and the interval from 492 to 540 Å in the second order. An additional mirror between the spectrometer grating and the detector allows observations at longer wavelengths that include the neutral hydrogen Lyα 1215.67 Å line (redundant channel). The UVCS slit, perpendicular to the Sunward direction on the plane of the sky, may be moved along the radial direction to observe the solar corona between 1.4 and 10 $R_\odot$, with a field of view of 40′, and, to cover all position angles, it can be rotated by 360° about an axis pointing to the center of the Sun. The detector pixel size corresponds to a spatial resolution of 7″ and a spectral resolution of 0.0993 Å (0.0915 Å pixel^{-1} for the redundant channel). For a complete description of the UVCS instrument, see Kohl et al. (1995).

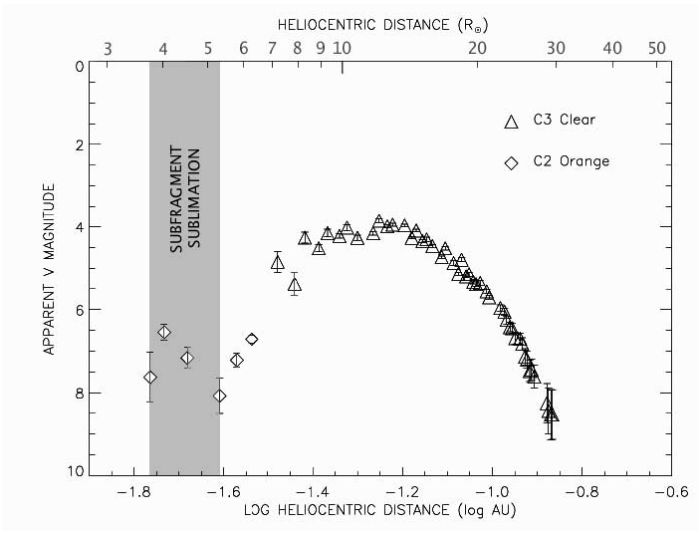

Fig. 2.—C/2001 C2 light curve as measured from LASCO C2 and LASCO C3 apparent visual magnitude. The secondary brightening after the main peak (∼12.1 $R_\odot$) has been interpreted as a possible fragmentation event that probably occurred farther from the Sun: if the fragment has a lower erosion rate than the main nucleus, it can be exposed in the final stage of the sublimation of the comet (*gray zone*).

Observations of comet C/2001 C2 were made when the comet was at heliocentric distances of 7.42, 6.17, 4.98, 3.60, and 2.20 $R_\odot$, as shown in Figure 1 (see Table 1 for the corresponding projected distances on the plane of the sky). At each heliocentric distance, we acquired a series of spectra with an exposure time of 200 s for a total observing time of about 70 minutes. To follow the comet's orbital motion, the position angle of the slit center was set equal to 110° for the first three heliocentric distances and 100° for the last two observations (see Fig. 1). The slit width was 150 μm wide, giving a field of view of 42″ (the projected slit width) by 40′ (the projected slit length); data were acquired with a spatial resolution of 21″ (which corresponds to a projected distance on the plane of the sky of ≃15,200 km) and a spectral resolution of 0.595 Å (0.549 Å for the redundant channel) given by the 150 μm slit width. The selected spectral windows covered the ranges 1024.3–1039.4, 997.2–1000.4, 989.3–992.9, and 975.8–986.8 Å (1211.1–221.1 Å for the redundant channel). These windows allow observations of coronal plasma in the lines of the O VI $\lambda\lambda$1032, 1037 doublet, of the Si XII λ499 line (second order), and of the H I Lyα and Lyβ lines. The 975.8–986.8 Å window includes the C III λ977 line, which allows us to estimate the amount of scattered light in the coronal spectra; this line may possibly be present in cometary spectra as well. Moreover, the 989.3–992.9 Å window (1205.4–1208.7 Å for the redundant channel) includes a blend of the N III λ991.6 and Si III λ1206.5 lines, also possibly present in cometary spectra.

The UVCS line emission at the time of the comet passage originates from a superposition of the cometary signal, the coronal and interplanetary emission (which might be important for the Lyα line), and the detector dark counts. Hence, the identification of the cometary signal was made by calculating the average emission over exposures taken before the comet entered the UVCS field of view (see Table 1) and subtracting this background from the following exposures. The comet emitted a signal only at 4.98 and 3.60 $R_\odot$; moreover, in the above spectral ranges the cometary emission was mainly observed in the H Lyα line. A transient weak emission was also detected in the Lyβ line and in the N III–Si III window. Unfortunately, the Lyβ intensity was very low and was used only to estimate the Lyα and Lyβ percentage due to radiative and/or collisional excitation (see below). In the N III–Si III window, we identify the observed emission as Si III λ1206.5 rather than N III λ991.6 or O I λ990.8, which fall somewhat off the wavelength observed. As we show in Figure 3, shortward of the Lyα peak, we see an

TABLE 2
ORBITAL PARAMETERS

Name	t_{peri}	q	e	ω	Ω	i	MPEC
C/2001 C2[a]	2001 Feb 7.92	0.0053	1.0	86.45	8.15	144.61	7580 2001-C09
C/2001 C3[a]	2001 Feb 4.98	0.0051	1.0	79.54	1.02	144.59	7582
C/2001 B3[a]	2001 Jan 25.36	0.0077	1.0	85.46	7.10	144.54	7573 2001-B45
C/2000 B5[a]	2000 Jan 18.87	0.0054	1.0	82.17	2.86	144.21	7386 2000-F34
C/1999 V2[a]	1999 Nov 8.50	0.0049	1.0	85.09	6.55	144.56	7517 2000-V22
C/2001 C4[b]	2001 Feb 8.44	0.0051	1.0	57.39	328.00	134.29	7582 2001-D42

[a] Kreutz sungrazers likely involved in fragmentation events with C/2001 C2.
[b] Sungrazer (C/2001 C4) not involved in fragmentation events with C/2001 C2.

intensity of about 7 times the background, which we ascribe to the Si III λ1206.5 line. This emission is not a fluctuation in the Lyα wing intensity, as it rises above background more than 3 σ. This interpretation is possibly supported by a background Lyα emission in our data (see § 4.2), due to interaction between cometary silicate dust grains and coronal plasma; hence, it is likely that the detected counts are due to Si III ions coming from the sublimation of silicate grains.

Because in our data no C III signal was recorded, no correction has been made for scattered light from the solar disk. We note that the C III λ977 line was observed by UVCS in spectra of comet Kudo-Fujikawa (Povich et al. 2003) and was ascribed to carbon atoms that evaporated from the dust and then photoionized. This process may be analogous to the process that we invoke to account for the Si III λ1206.5 line in our spectra. In the following, we focus on the cometary emission at 4.98 and 3.60 $R_\odot$ in the Lyα line.

In Figure 4 we show composite images of the integrated Lyα intensity, from all the available exposures at the two heliocentric distances. These images have been scaled in arcseconds in the direction normal to the slit, taking into account the cometary velocity component perpendicular to the slit $v_\perp$ and the duration of each exposure. They give a realistic representation of the comet's appearance, provided there are no major changes in the comet during the time it takes to cross the UVCS slit. The left panels (i.e., before the subtraction of background Lyα) show that at 4.98 $R_\odot$ the comet is adjacent to a weakly emitting coronal structure, which is crossed by the comet at 3.60 $R_\odot$. This very small coronal feature was observed in the UVCS Lyα intensity at 2.20, 3.60, and 4.98 $R_\odot$ but is hardly detectable in the LASCO C2 image (see Fig. 1). In the 3.60 $R_\odot$ panels in Figure 4 (*top*), because of the low intensity of the coronal background with respect to the cometary signal, the Lyα intensity has been plotted on a logarithmic scale to show both the coronal and cometary emission.

A comparison between the top and bottom panels of Figure 4 reveals a very interesting difference between the comet structure at 4.98 and 3.60 $R_\odot$: at the greater heliocentric distance, the image shows two tails, only one of which is observed at the lower altitude (we hereafter refer to the northernmost and

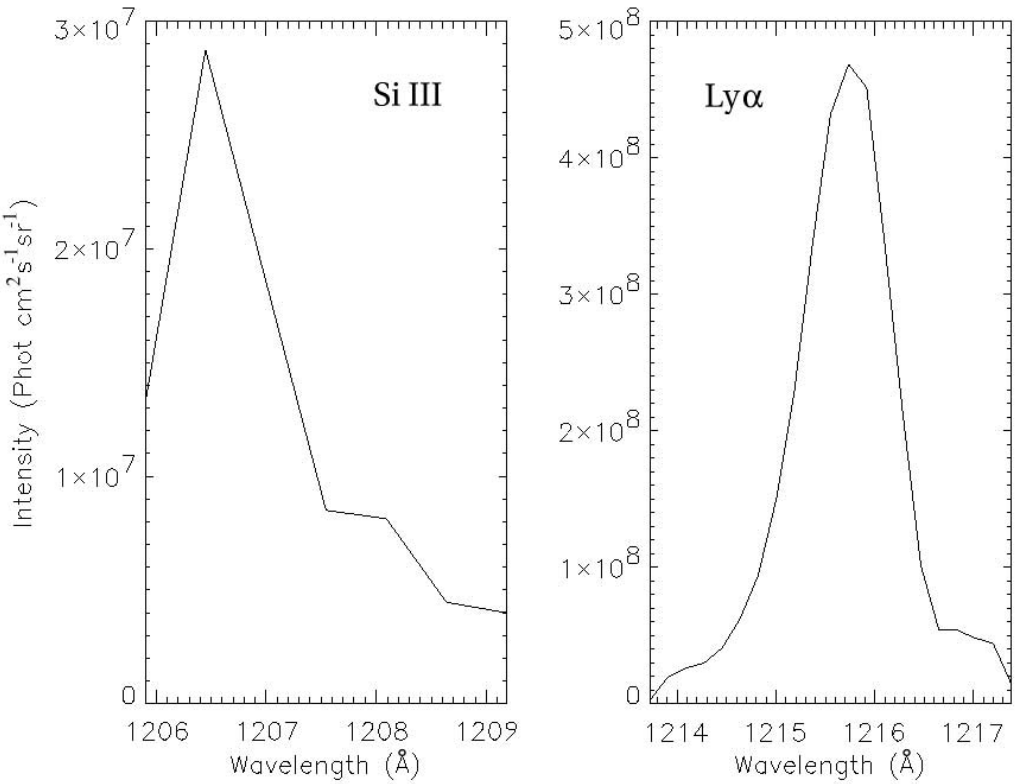

FIG. 3.—Line profiles for the Si III (*left*) and the Lyα lines (*right*) at 4.98 $R_\odot$ (average over three exposures).

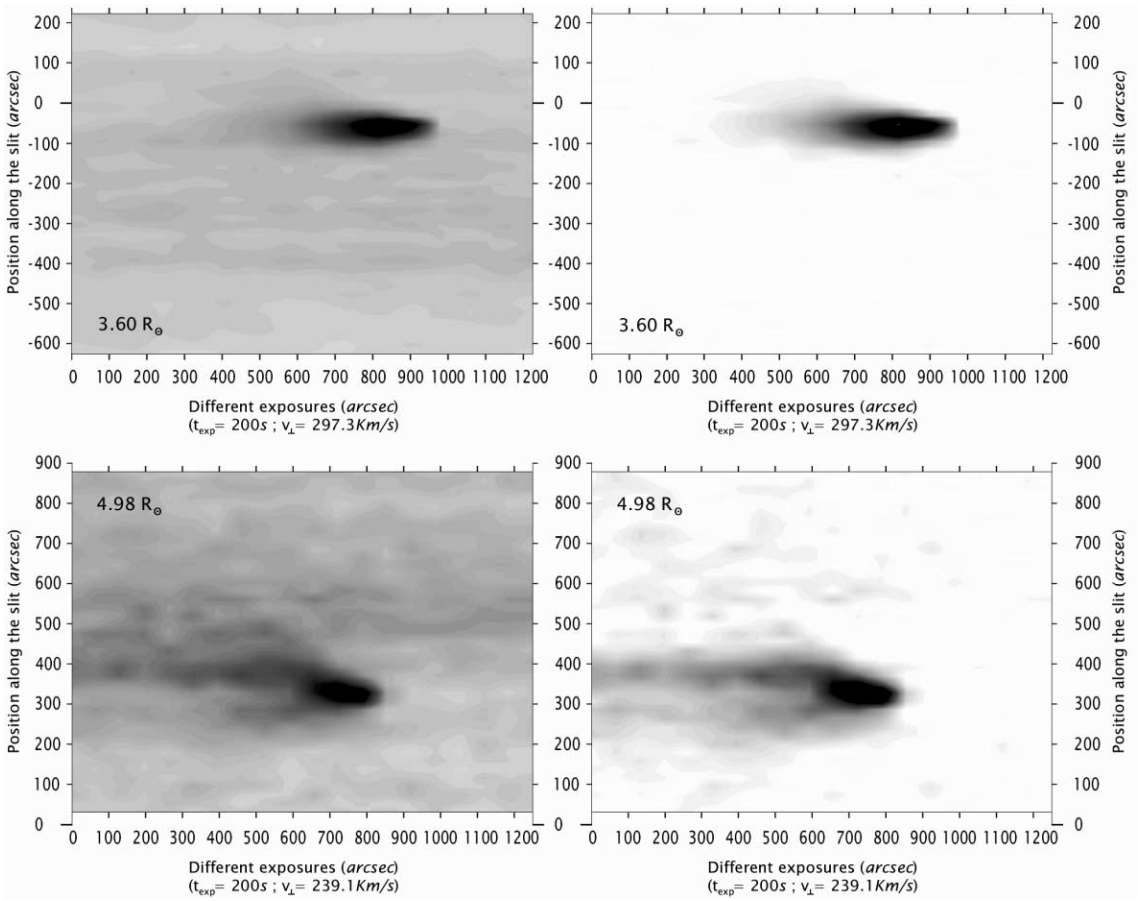

FIG. 4.—Composite Lyα images of C/2001 C2 observed at 3.60 (*top*) and 4.98 $R_\odot$ (*bottom*). At both heliocentric distances we give the Lyα images before (*left*) and after (*right*) the subtraction of the background Lyα. Note at 4.98 $R_\odot$ the two tails and the longer Lyα signal persistence after the comet passage with respect to the 3.60 $R_\odot$ observation. In the *y*-axis 0 marks the UVCS slit center position; north is up. These images have not been corrected for the cometary motion along the slit.

brighter tail as tail 1, tail 2 being the weaker structure). In addition, at 4.98 $R_\odot$ the main tail intensity seems to decrease with time (or distance) more slowly than does the single tail at 3.60 $R_\odot$. A first interpretation of the data is that the comet is composed of two fragments at 4.98 $R_\odot$ and of a single object at 3.60 $R_\odot$. Nevertheless, three other interpretations for the origin of the two tails are possible. First, the two tails could be generated by a single object, if one hypothesizes that on the surface of the nucleus are two emitting regions that eject plasma and dust. However, we have to consider that, for sungrazing comets, because of the small heliocentric distances, the nucleus is exposed to an extremely high solar flux ($\sim 2.5 \times 10^9$ ergs cm^{-2} s^{-1} at 5 $R_\odot$); hence, it is difficult to imagine a nucleus with only two emitting regions: probably the whole surface of the nucleus would be active, and this interpretation can be excluded. A second possible interpretation is that cometary dust particles were ejected from a single object at two different times: model computations (Z. Sekanina 2004, private communication) show that the sector in which dust ejected from the comet at different times should point is between S1° and S15° latitude, and the two tails in Figure 4 are approximately located between S4° and S12°, hence, in exactly the same sector. In this case, tail 1 would be the younger emission, made up mostly of submicron-sized grains, while tail 2 would be the older emission, containing (at the observed distances of up to $\sim 200''$) relatively large particles. In principle, we cannot exclude this second interpretation of the origin of the two tails; however, under this interpretation, it is not easy to explain why the comet shows two tails at 4.98 $R_\odot$ and only one tail $\sim$1 hr later, at 3.60 $R_\odot$ (see Fig. 4). A third interpretation of the origin of the two tails is that the enhanced Lyα emission close to the small coronal streamer (tail 1) originates from the interaction between the cometary plasma and the streamer itself; we rule out this possibility in § 4. In conclusion, in this study we concentrate only on the two-fragment interpretation, assuming that the two observed tails are the signatures of two separate fragments.

To separate the contributions of the two tails, we assume that the cometary Lyα intensity distribution along the slit is symmetric around the peak, as suggested by the image at 3.60 $R_\odot$. After correcting the Lyα image for the cometary motion in the direction parallel to the slit (using the value of the velocity component $v_{\rm slit}$ given in Table 1), we assumed that the tail 1 intensities northward of their peak values at each time are unaffected by tail 2, and we built the intensity distribution of tail 1 by simply mirroring its northern isophotes (Fig. 5, *middle*). The secondary tail isophotes were obtained by subtracting from the original Lyα image (Fig. 5, *left*) the contribution of tail 1 (Fig. 5, *right*). We note here that with this procedure the number of Lyα counts we attribute to tail 1 and/or to tail 2 depends also on the subtraction of the coronal background: in particular, the intensity of the small coronal streamer mentioned above can slightly change during the observation. For instance, an underestimate of the streamer intensity, which lies northward of tail 1,

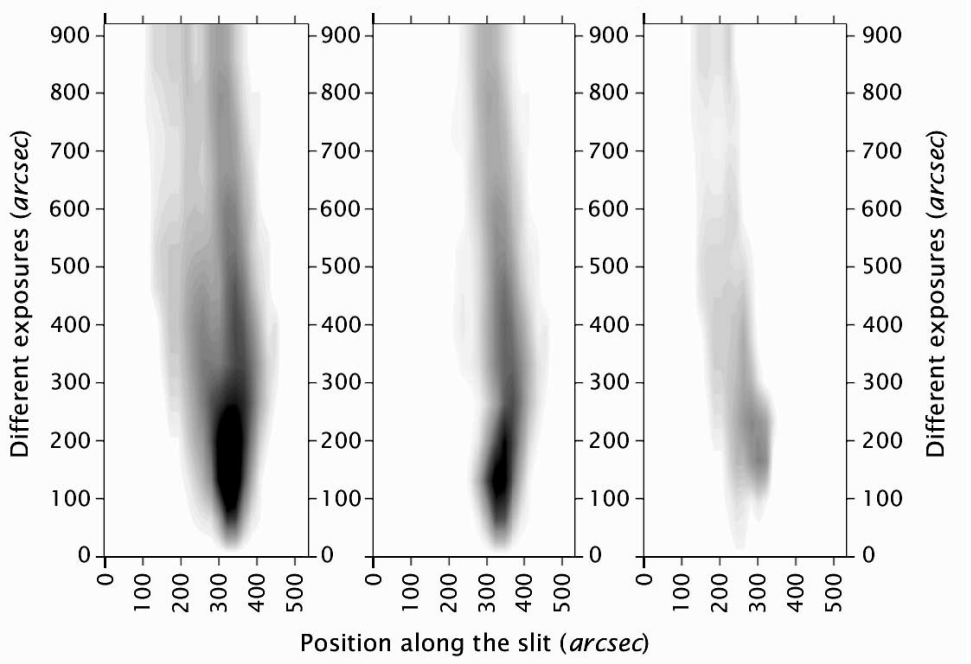

FIG. 5.—*Left*, Composite Lyα image of C/2001 C2 observed at 4.98 $R_\odot$ and shifted for the cometary motion along the slit (north is on the right); *middle and right*, tail 1 and tail 2 Lyα images obtained, respectively, by symmetric reflection of the northern half of tail 1 and by subtraction of the tail 1 isophotes from the observed image (see text).

could lead to an overestimate of the Lyα counts in tail 1, hence, by reflection and subtraction, an underestimate in tail 2. However, as we verified by performing the same analysis with different values of the streamer intensity, this indeterminacy can lead to a systematic error of about 30% over all the derived parameters. Hence, the errors we give in the following sections are only statistical errors from the fit (see later); the systematic error mentioned above must also be considered.

2.3. *Cometary and Coronal* Lyα *Line Profiles*

We now proceed to analyze the Lyα line profiles for the coronal and cometary signals. To this end, we made a Gaussian fit to the Lyα profiles obtained at the position along the slit where the line intensity peaks. Average coronal profiles were obtained by summing over all the exposures prior to the comet arrival and over all the bins for which we later observed a cometary signal. This coronal background was subtracted from the cometary signal before fitting the comet line profiles.

Table 3 gives the parameters derived from the Gaussian fits to the cometary and coronal Lyα profiles. As we mentioned, the Lyβ line signal was too weak to allow us to derive a statistically significant profile. The FWHM from the Gaussian fit has been corrected for the instrumental profile; from the corrected FWHM (i.e., FWHM$_c$ in Table 3) we derived the kinetic temperature T_k.

As observed also by Uzzo et al. (2001) for comet C/2000 C6, at 4.98 $R_\odot$ the shift $\Delta\lambda$ between the cometary and coronal profile (or, more precisely, the shift $\Delta\lambda = \lambda_c^{\rm com} - \lambda_c^{\rm cor}$ between the centroids of the coronal and cometary line profiles) in the first exposure is significant. This shift can be ascribed to partial filling of the UVCS aperture by the comet, which results in a profile shifted toward longer wavelengths.

TABLE 3

Lyα LINE PROFILE PARAMETERS FROM GAUSSIAN FITS

h ($R_\odot$)	$t_{\rm exp}$ (UT)	$\Delta\lambda$ (Å)	FWHM (Å)	FWHM$_c$ (Å)	T_k (10^6 K)	I(Lyα) (photons cm^{-2} s^{-1} sr^{-1})
			Cometary Lyα Profile			
4.98.....	19:18	0.260	1.166	1.016	1.37	3.349×10^9
	19:22	0.131	1.119	0.9611	1.23	3.095×10^9
	19:25	0.123	1.123	0.9661	1.24	2.401×10^9
	19:28	0.121	1.034	0.8602	0.983	1.157×10^9
3.60.....	20:18	0.114	1.087	0.9231	1.13	3.839×10^{10}
	20:21	0.0621	1.001	0.8211	0.896	5.116×10^{10}
	20:25	0.0402	1.045	0.8740	1.01	2.491×10^{10}
	20:28	0.0561	1.032	0.8587	0.980	1.307×10^{10}
			Coronal Lyα Profile			
4.98.....	18:54–19:18	...	0.9325	0.7356	0.719	9.714×10^8
3.60.....	20:04–20:18	...	1.042	0.8706	1.01	4.841×10^9

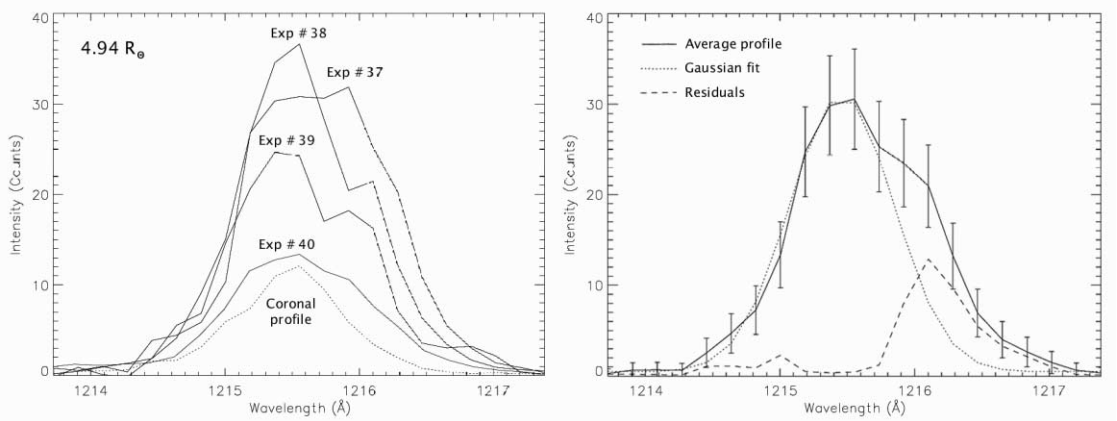

FIG. 6.—*Left*: Cometary Lyα line profiles at 4.98 $R_\odot$ (*solid line*; coronal profile subtracted) for the first four exposures after the comet entered the UVCS slit. The shape of the Lyα profile in first exposures may be interpreted as a superposition of two profiles (see text): the redshifted one disappears after the fourth exposure, and the cometary line approaches the coronal profile (*dotted line*). *Right*: Cometary profile averaged over the first three exposures (*solid line*), Gaussian fit over the main component (*dotted line*), and the secondary profile (*dashed line*).

Table 3 shows that at 3.60 $R_\odot$, the width of the Lyα profile from the comet is the same as the coronal width. This means that the coronal plasma and the plasma emitting the cometary signal have the same temperature, an effect that is discussed in § 3 and agrees with the results obtained by Uzzo et al. (2001) in his observations of the sungrazing comet C/2000 C6. Because at 3.60 $R_\odot$ we are sampling coronal plasma from a weakly emitting filamentary structure, we may compare the temperature that we derived with typical streamer values: for instance, Strachan et al. (2002) found at 3.60 $R_\odot$ a perpendicular kinetic temperature for Lyα of $(1–2)\times10^6$ K along the streamer axis, in agreement with our value.

At 4.98 $R_\odot$, Table 3 suggests that the cometary Lyα profile is wider than the coronal profile at that heliocentric distance, but, as shown by a more sophisticated study, there are two components to the profile. For a detailed analysis of the line profiles at this heliocentric distance, we built the Lyα profiles for tail 1 over the bin with peak Lyα intensity from each of the first four exposures after the comet entered the UVCS slit. These are given in Figure 6 (*left*). The figure shows that a secondary Lyα peak, redshifted with respect to the main component and weakening progressively with time (it can hardly be identified after the fourth exposure), may be present in the first exposures. To increase the statistical significance of the secondary profile, if any, we averaged the Lyα profile over the first three exposures (see Fig. 6, *right*). Superposed onto this, we also show a Gaussian fit to the main component: the fit has been constructed by taking into account only the blue side of the line and assuming the profile to be symmetric around its peak. The profile of the secondary component, calculated from the difference between the observed and the Gaussian predicted intensities, is also shown. Bars on the figure represent the 1 σ error bars; intensities of the secondary component are above the 1 σ uncertainty level. We conclude that a possibly significant secondary redshifted Lyα component is present in the first four exposures after the comet entered the UVCS slit. The identification of two components in the Lyα line profile has been possible only in tail 1, because of the lower intensity measured in the secondary tail profiles; however, the Lyα profiles observed in tail 2 also appear to be wider than the coronal profile, suggesting that this secondary Lyα component is present in both tails. In the following, we consider the Lyα profile at 4.98 $R_\odot$ to be the sum of two components: the origin of the secondary component and the 0.6 Å relative Doppler shift are discussed in § 3.2.

The FWHM of the main component of the Lyα profile (Fig. 6, *right*, *dotted line*) is about 0.9 Å, hence, consistent with the coronal width evaluated from the precomet exposures (see Table 3). Because at this heliocentric distance we are in a low-latitude open-field region, we should compare the value that we found with values given in the literature for the Lyα width in low-latitude coronal holes. However, there are no Lyα width values for low-latitude coronal holes in the literature, and since at 4.98 $R_\odot$ the field lines of coronal streamers are probably open, we can compare our values with those of Kohl et al. (1997) and Frazin et al. (2003), who found in an equatorial coronal streamer at 5 $R_\odot$ a 1/*e* Lyα width corresponding to 1.5×10^6 K, in agreement with our value given in Table 3, $\sim1.2\times10^6$ K. Polar coronal hole measurements give the temperature $T_k\sim3.8\times10^6$ K above 4.0 $R_\odot$ (Cranmer et al. 1999), which is larger than that we observed in the comet.

3. PHYSICS OF Lyα EMISSION

3.1. *Cometary and Coronal Plasma Interactions*

For the convenience of readers, we recall briefly here the mechanisms for Lyα emission, originally suggested by Raymond et al. (1998) and Uzzo et al. (2001), to explain the enhanced Lyα emission from the interaction of the comet and coronal plasmas. The reader is referred to the above papers for a more detailed treatment of the problem.

First, we have to check whether the observed Lyα line is radiatively excited or has a significant collisional component. In general, for the hydrogen Lyα and Lyβ lines, it is possible to separate the two components by solving a simple linear system that requires the collisional and radiative Lyβ/Lyα ratios to be known (in the following, $R_{\beta\alpha,c}$ and $R_{\beta\alpha,r}$; see, e.g., Marocchi et al. 2001). These ratios depend on well-known atomic factors; $R_{\beta\alpha,c}$ depends also on the electron temperature T_e, while $R_{\beta\alpha,r}$ depends on the Lyα and Lyβ disk intensities and on the chromospheric and coronal line width. At the high temperatures typical of coronal plasma ($\log T_e\sim6.0$) $R_{\beta\alpha,c}\simeq0.14$, while using $I_{\rm disk}({\rm Ly}\alpha)=6.678\times10^{15}$ photons cm^{-2} s^{-1} sr^{-1} from SOLSTICE data and $I_{\rm disk}({\rm Ly}\beta)=9.947\times10^{13}$ photons cm^{-2} s^{-1} sr^{-1} from SUMER data, both measured on 2001 May 14 (the SUMER observation closest in time to our observations), we computed $R_{\beta\alpha,r}\simeq0.0021$. From these values, it turns out that at both 3.60 and 4.98 $R_\odot$ about 100% of cometary Lyα originates from radiative excitation of neutral hydrogen,

while the Lyβ radiative component is only $\sim$30% of the total emission.

Hence, because the cometary Lyα line is only radiatively excited (as is usually the case in the corona; see, e.g., Raymond et al. 1997) and, as we show in § 2.3, its width is not larger than the coronal line width, we can invoke two possible explanations of its origin: either the enhanced Lyα intensity originates from photons scattered by hydrogen atoms created in the photodissociation of the water molecules ejected by the comet or else the products of water dissociation interact with coronal protons and, by charge transfer processes, create neutral hydrogen atoms with the same kinetic temperature as the coronal protons, which then scatter Lyα line photons.

To identify the origin of the cometary Lyα emission, we point out that the Lyα signal from the products of dissociation of water would have a profile narrower than the coronal one and disappear shortly after the comet leaves the UVCS slit (Raymond et al. 1998). As we show in § 2.3, the cometary profiles have the same width and the same centroid position as the average coronal profile; hence, the second-generation neutral hydrogen atoms have the same bulk speed and kinetic velocity distribution as those of the coronal H atoms. We conclude that the H atoms responsible for this emission formed from the interaction of coronal protons with neutral atoms that are secondary products of the comet ejection of H_2O. In fact, because in the process $p^+ + H \rightarrow H + p^+$ the momentum transfer is very small (McClure 1966), the newly formed H atoms have about the coronal proton velocity distribution. This conclusion agrees with previous findings by Uzzo et al. (2001) from the analysis of the sungrazer C/2000 C6.

3.2. *Origin of the Secondary Lyα Component at* 4.98 $R_\odot$

We can now discuss the origin of the secondary component observed at 4.98 $R_\odot$ in the Lyα profiles of tail 1, which we described in § 2.3. The secondary profile is observed only in the first four exposures, which correspond to a total time of 800 s, i.e., about the same value we find (see § 4.1) from the model for the characteristic time τ_{cx} for the charge exchange process discussed above. Hence, while the main profile is due to Lyα photons scattered by H atoms created by charge transfer with coronal protons (which are at rest with respect to coronal H atoms), we suggest that the secondary profile originates from those H atoms, created by H_2O photodissociation, that did not have enough time for charge exchange and, moving with the comet along the line of sight (LOS), produce a redshifted profile. This hypothesis is supported by the narrow width ($\sim$0.5 Å) of the secondary profile shown in Figure 6: because the cometary material is "cooler" than the coronal plasma, the line has a smaller width. However, the shift of about 0.6 Å between the main and the secondary Lyα profile in Figure 6 (corresponding to about 150 km s^{-1}) is larger than that implied by the component $v_{LOS} \sim 80$ km s^{-1} of the cometary velocity derived from the orbital parameters given in the MPEC (see Table 1). This inconsistency may be due to the uncertainty in separating the two components of the Lyα profile.

In this scenario, we may also explain why this secondary component is unobservable at 3.60 $R_\odot$: at 4.98 $R_\odot$ the comet is crossing a coronal hole region; hence, the secondary Lyα intensity due to the H atoms moving inward with the comet ($v_r \sim$ 250 km s^{-1}) and the main component due to the H atoms moving outward with the solar wind ($v_{out} \sim 170$ km s^{-1}) are both Doppler dimmed. On the contrary, at 3.60 $R_\odot$ the comet is crossing a coronal streamer; hence, only the secondary Lyα component due to the H atoms from water photodissociation is Doppler dimmed, while the main component comes from coronal H atoms with $v_{out} \sim 0$. As a consequence, the expected ratio between the intensities of the two components is $\sim$20, making the secondary component unobservable. A possible objection to this interpretation comes from the kinetic temperature that we derived from the secondary profile ($T_k \sim 2.5 \times 10^5$ K), higher than that expected for cometary material.

An alternative explanation for the secondary Lyα component must be considered: the O atoms from the H_2O photodissociation have a cross section for the charge exchange process with coronal protons that is about the same as the H atoms charge exchange cross section (see, e.g., Kimura et al. 1997), because the H and O first ionization potentials are approximately equal. This means that H atoms could form also by charge transfer with cometary O atoms, but, because O is about 16 times heavier than H, some momentum may be exchanged in the process. This might explain the redshift of the secondary component: because of the near equality of the cross sections for the two processes, we can assume that the number N_{Hp} of H atoms created by charge transfer between cometary H atoms and coronal protons is about twice the number N_{HO} of H atoms created by the same process with cometary O. Hence, assuming that these atoms are responsible for the secondary Lyα emission, we estimated that, to reproduce its intensity, each H atom scatters $\bar{g} = 0.62$ Lyα chromospheric photons s^{-1}. At 4.98 $R_\odot$ in a static plasma, we have $\bar{g} = 4.50$ photons s^{-1} H^{-1}; hence, we need a Doppler-dimming factor of 0.14 to bring $\bar{g}$ down to the value 0.62 that we estimated. This corresponds to a plasma speed of $\simeq$260 km s^{-1} (see Kohl et al. 1997), in agreement with the cometary radial velocity v_r (see Table 1). The explanation we gave above for the absence of the secondary component at 3.60 $R_\odot$ holds also for this alternative explanation. However, an objection to this interpretation comes from Lindsay et al. (1996), who seem to imply that very little momentum transfer occurs in the charge exchange between O atoms and coronal protons.

A third possibility is that the comet produces enough gas to dynamically affect a small region of the corona that it passes through. This can take the form of a bow shock (e.g., Raymond et al. 1998). The comet produces about 10^{28} atoms s^{-1} at 4.95 $R_\odot$, comparable to the number of atoms swept up per second in a cylinder of 10^{10} cm radius (approximately the mean free path for charge transfer) and length given by the comet motion in 1 s, if the coronal density is in the range estimated below. Thus, the cometary material can dynamically affect the coronal gas, but it is not clear whether or not a bow shock forms. We are unable to chose among the interpretations that we outlined, and we leave this point open for future work.

4. MODEL

We now show how the observed intensities allow us to derive the comet outgassing rate and the dimension of the cometary nucleus. To this end, we need to establish a relationship between the unknown number $\dot{N}$ of neutral H atoms produced by cometary outgassing and the observed Lyα intensity. The mean lifetime τ_H of H atoms produced by photodissociation may be written as

$$\tau_H = (\tau_{cx}^{-1} + \tau_{ion}^{-1})^{-1}, \quad (1)$$

where the charge transfer rate τ_{cx}^{-1} and the ionization rate τ_{ion}^{-1} depend on the plasma conditions and are in general unknown; these rates increase as the comet approaches the Sun. However, for plasma conditions at 3.60 $R_\odot$ (temperature of $\sim 10^6$ K and

relative velocity between coronal gas and cometary H atoms of about 250 km s^{-1}), it turns out that

$$\tau_{cx} = \tau_{ion} \simeq \frac{3.1 \times 10^7 \text{ cm}^{-3} \text{ s}}{N_e} \Rightarrow \tau_H = \frac{\tau_{ion}}{2} \quad (2)$$

(Scholz & Walters 1991; Uzzo et al. 2001). At 4.98 $R_\odot$, the relative velocity between coronal plasma and cometary H atoms increases because of the coronal plasma outflow velocity: for a low-latitude coronal hole outflow velocity $v_{out} \simeq 170$ km s^{-1} (Poletto et al. 2002), we have a relative velocity of about 420 km s^{-1} and $\tau_{cx} \simeq 1.8 \times 10^7$ cm^{-3} $s/N_e = \tau_{ion}/R_\tau$ ($R_\tau \equiv \tau_{ion}/\tau_{cx} = 1.72$). Hence, in general, $\tau_H = \tau_{ion}/(R_\tau + 1)$ with $R_\tau = 1$ and $R_\tau = 1.72$, respectively, at 3.60 and 4.98 $R_\odot$. The number N_{com} (cm^{-3}) of neutrals moving with the comet and outgassed at a rate $\dot{N}$ (cm^{-3} s^{-1}) is $N_{coma} = \dot{N}\tau_H = \dot{N}\tau_{ion}/(R_\tau + 1)$. These atoms undergo charge transfer with coronal protons at a rate of τ_{cx}^{-1}; hence, the comet, moving at velocity v, leaves along its path a number $N_H = N_{com}/(\tau_{cx}v) = \dot{N}R_\tau/[(R_\tau + 1)v]$ of neutrals per centimeter. This shows that N_H is independent of the electron density N_e, because an increase in N_e corresponds to a greater number of neutrals created by charge transfer: these, however, have a shorter lifetime because of the increase of the ionization rate. After the comet passage, the Lyα starts decreasing with time: the number N_H of H atoms that the comet leaves along its path via charge transfer decays exponentially with a lifetime of τ_{ion}, and the cometary Lyα signal disappears. Changes in N_e modify only the exponential decay $e^{-t/\tau_{ion}} \sim e^{-tN_e/k}$ ($k = 3.1 \times 10^7$ cm^{-3} s), giving a longer Lyα signal persistence when N_e is smaller.

As we anticipate in § 2.2, at 4.98 $R_\odot$ the Lyα isophotes show two cometary tails (see Fig. 4). Now from equation (2) we can exclude the possibility that the enhanced emission, dubbed tail 1, is due to the interaction between the cometary plasma and the enhanced density of the coronal streamer. Where the electron density N_e increases (i.e., near the streamer's edge), the charge transfer rate τ_{cx}^{-1} increases and the number of H atoms produced (hence, the Lyα intensity) should increase. Nevertheless, as a consequence of equation (2), at locations where N_e rises, the Lyα signal duration decreases, leading to a weaker rather than a stronger Lyα emission at the location of tail 1 in Figure 4. Moreover, sublimation of cometary dust grains provides a better explanation of the persistent Lyα signal, as is shown in § 4.2.

The total (i.e., summed over the slit length) number of Lyα counts C_i expected in the exposure i after the first cometary observation in the spectrograph slit (see Uzzo et al. 2001) is

$$C_i = \frac{A_{eff}}{4\pi\delta^2}\frac{\dot{N}\bar{g}}{v}\frac{R_\tau}{R_\tau + 1}\int_{it_{exp}}^{(i+1)t_{exp}}\int_0^l e^{-[t-t_{crs}(x)]/\tau_{ion}}\, dx\, dt, \quad (3)$$

where A_{eff} is the effective area of the UVCS instrument ($A_{eff} = 0.0075$ and 0.015 cm^2, respectively, at the projected heliocentric distances of 3.44 and 4.94 $R_\odot$), δ and v are given in Table 1, $t_{exp} = 200$ s is the exposure time, $l = 3.0 \times 10^9$ cm is the UVCS slit width projected onto the plane of the sky, $t_{crs}(x) = t_{st} + x/v$ is the time at which the comet crosses the position x on the slit (t_{st} is the unknown time at which the comet first enters the slit) and τ_{ion} is the unknown characteristic time for H atom ionization. In this model there are two unknown parameters (τ_{ion} and t_{st}) and a normalization $\dot{N}$: it is possible, given the observed C_i curve, to find the pair of values for (τ_{ion}, t_{st}) at which the χ^2-value is minimum: statistical errors in the fit are estimated from the iso-χ^2 curves (see Fig. 8). We note that we can easily estimate the electron density N_e of the plasma encountered by the cometary nucleus simply from the τ_{ion}-value given by the fit.

The value of $\bar{g}$ has been computed from the following parameters: at 3.60 $R_\odot$, we used the average $T_k = 1.0 \times 10^6$ K from cometary profiles (Table 3) and, since the comet is passing through a small streamer, an outflow speed of $v_{out} = 0$ (see, e.g., Strachan et al. 2002); at 4.98 $R_\odot$, we used $T_k = 7.19 \times 10^5$ K from the coronal FWHM (see Table 3) and the outflow speed estimated above from Poletto et al. (2002). For a scattering angle of $\theta_{sct} = 90^\circ$ (the comet was approximately in the plane of the sky at both heliocentric distances; see δ-values in Table 1), we obtained $\bar{g} = 8.62$ photons s^{-1} H^{-1} at 3.60 $R_\odot$ and $\bar{g} = 1.09$ photons s^{-1} H^{-1} at 4.98 $R_\odot$. At both heliocentric distances, we used $I_{disk}(\text{Ly}\alpha) = 7.75 \times 10^{15}$ photons cm^{-2} s^{-1} sr^{-1} from the 2001 February 7 SOLSTICE measurement.

The outgassing rate $\dot{N}$ derived from the model can be used to estimate the ejected mass rate Q_{H_2O} (kg s^{-1}) by simply assuming that each water molecule gives rise to two neutral hydrogen atoms. O atoms can also neutralize protons by charge transfer, but oxygen is ionized more rapidly than hydrogen. From the $\dot{N}$-value, it is possible also to give an estimate of the active surface S_{act} of the cometary nucleus exposed to the solar radiation: assuming a balance between the energy supplied by the solar radiation over S_{act} and the energy required to sublimate the quantity of ice derived from $\dot{N}$, we have

$$S_{act} = \frac{\dot{N}L}{F_\odot(1 - A)N_A}, \quad (4)$$

where $L = 4.81 \times 10^{11}$ ergs mol^{-1} is the latent heat of sublimation of ice, $A = 0.06$ is the cometary albedo, $F_\odot = 1.37 \times 10^6 (215.21\ R_\odot/r)^2$ ergs cm^{-2} s^{-1} is the solar flux scaled to the cometary heliocentric distance $r(R_\odot)$ (see Table 1), and N_A (molecules mol^{-1}) is Avogadro's number. From the S_{act}-value, it is possible (assuming a spherical nucleus) to estimate the equivalent radius for the cometary nucleus $R = (S_{act}/\pi)^{1/2}$. This relationship holds only in the absence of unobserved fragmentation events.

4.1. *Model Results at* 4.98 $R_\odot$

Before discussing the model results at 4.98 $R_\odot$, we note here that, whatever interpretation we give to the secondary Lyα profile (§ 3.2) observed at this heliocentric distance, the H atoms responsible for this secondary emission are not included in the model described above. Because the intensity of the secondary profile (see Fig. 6) is about 20% of the whole Lyα emission at 4.98 $R_\odot$, before applying the model to the observed profile of the Lyα counts versus time, this component was subtracted from the integrated Lyα intensity in exposures 37, 38, and 39 (see Fig. 6).

The derived C_i curves for tails 1 and 2 were compared with the C_i predicted curve (eq. [3]) to determine the fragment parameters. As we can see in Figure 7, the C_i curve for the secondary tail (*right*) was easily fitted, yielding the parameters given in Table 4. On the contrary, the tail 1 curve (*left*) shows a very slow decrease in time, and the fit gives us a very high τ_{ion}-value ($\tau_{ion} \geq 2000$ s^{-1}), hence, a low N_e ($\leq 1.6 \times 10^4$ cm^{-3}). As we mention in § 2.2, tail 1 is closer than tail 2 to a small coronal streamer, so in this region we expect an electron density equal to or greater than the density $N_e = 1.6 \times 10^4$ cm^{-3} obtained from the tail 2 fit. However, the shape of the tail 1 C_i curve (Fig. 7, *left*, *dashed line*) is not exponential and, rather than decreasing to 0 counts over the observed exposures, tends toward a constant Lyα emission of about 280 counts. Hence, to determine

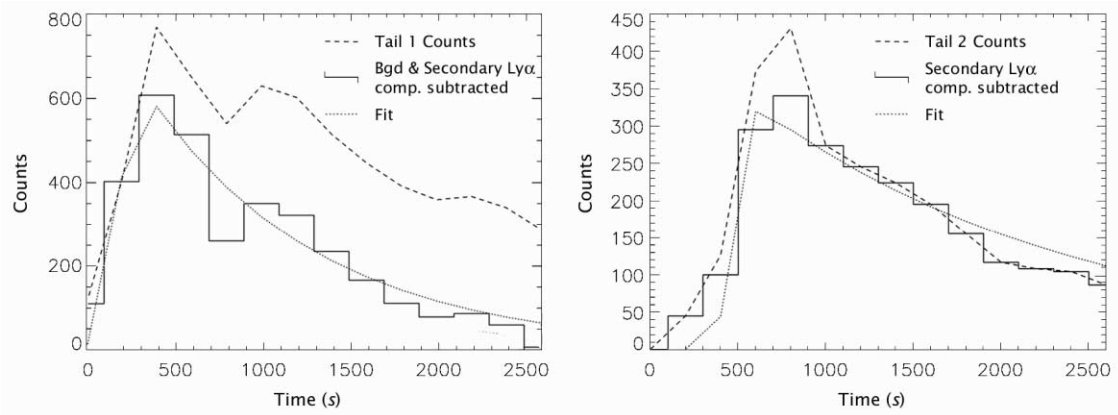

FIG. 7.—Observed (*solid line*) and modeled (*dotted line*) Lyα counts at 4.98 $R_\odot$ in the main (*left*) and secondary (*right*) cometary tail. Before fitting the observed counts, we subtracted from both tails the intensity of the secondary Lyα component (see text) from the first exposures; moreover, before fitting the counts of tail 1, a constant term of 280 counts was subtracted from the tail 1 curve to take into account the effect of pyroxene dust grains.

$\tau_{\rm ion}$, we subtracted a constant background of 280 counts from the measured intensities, obtaining the solid curve in Figure 7. From this curve, using the above model, we evaluated the main-fragment parameters given in Table 4 (the $t_{\rm ent}$-value given in Table 1 was computed from the main-fragment $t_{\rm st}$-value). As expected, the derived $\tau_{\rm ion}$-values in Table 1 decrease from tail 2 to tail 1, giving us a higher electron density near the small coronal streamer ($N_e = 3.0 \times 10^4$ cm^{-3}). We give a detailed interpretation for the constant Lyα in § 4.2: here we anticipate only that this Lyα emission is ascribed to the sublimation of pyroxene dust grains, a process that yields an extra number of neutrals in the coma. We note from Table 4 that the trailing fragment entered the slit 270 s after the main nucleus, which corresponds to a distance of $\simeq$66,420 km, assuming a projected velocity on the plane of the sky of $v_{\rm sky} \simeq v_r \simeq 246$ km s^{-1}. Along the slit, the two tails are separated by about 4 bins $\simeq 60,990$ km; hence, on the plane of the sky, we observed a distance between the main nucleus and the subfragment of $\simeq$90,170 km. This distance corresponds to about 124″ on the plane of the sky: because the LASCO C3 pixel resolution (equivalent to the size of 2 pixels) is 112″, if we take into account that the fragment is probably fainter than the main nucleus, it is likely that the two objects are not resolved in white-light images, as anticipated in § 2. From the $S_{\rm act}$-values, assuming a spherical shape for both the main and the secondary fragment, we obtained, respectively, radii of $7.8^{+0.4}_{-0.5}$ and $5.4^{+0.2}_{-0.5}$ m; these values are similar to the diameters of the nuclei given by Uzzo et al. (2001) for comet C/2000 C6.

4.2. *Effect of Pyroxene Dust Grains*

We have shown in § 4.1 that, at 4.98 $R_\odot$, a subtraction in each exposure of a constant Lyα intensity of about $I({\rm Ly}\alpha) \simeq 280$ counts $= 3.93 \times 10^9$ photons cm^{-2} s^{-1} sr^{-1} from the tail 1 C_i profile allows us to determine by the model described above a realistic $\tau_{\rm ion}$-value. The additional number $\bar{N}_{\rm H}$ of H atoms that produces this Lyα emission is $\bar{N}_{\rm H} = [4\pi I({\rm Ly}\alpha)]/\bar{g}L \simeq 3.0$ H cm^{-3}, where $\bar{g}$ has been computed in § 4 and L is the extension of tail 1 along the LOS, which we assume to be of the same order as its extension on the plane of the sky ($L \simeq 10$ bins $\simeq 1.52 \times 10^5$ km; see Fig. 5, *middle*). We need now to explain the origin of these additional H atoms.

As we noted in § 1, Kimura et al. (2002) interpreted the observed sungrazer light curves in terms of the different characteristic timescales for sublimation of olivine and pyroxene dust grains. These authors defined the dust sublimation zone as the heliocentric distance at which the timescale for grain sublimation τ_s is equal to the time $\tau_{\Delta r}$ taken by the comet to cover the distance $\Delta r = 0.1\ R_\odot$. They found pyroxene aggregates in sungrazer comae to have their sublimation zone at $h \sim 5\ R_\odot$, which corresponds to the heliocentric distance of our observations. Moreover, Kimura et al. (2002) hypothesize that "the sublimation of pyroxene grains might account for the Lyα emission that peaks around 4–5 $R_\odot$ if pyroxene grains act as agent to neutralize protons in the solar corona." In the following, we show how the additional number of H atoms evaluated above can be explained in terms of a pyroxene dust grain density, and we give an order-of-magnitude estimate of its value. From a study of nine sungrazer dust tails, Sekanina (2000) found that the orientation of dust tails matches remarkably well a synchrone (i.e., the locus of the dust grains of different sizes ejected at the same time) if on average the peak production occurs at the ejection time $t_{\rm ej} \simeq 1.1$ days before perihelion. If we assume this value for $t_{\rm ej}$, the time Δt between the dust ejection and

TABLE 4
C/2001 C2 MODEL AND DERIVED PARAMETERS

MODEL PARAMETERS				DERIVED PARAMETERS			
$R_{\rm sky}$ ($R_\odot$)	$t_{\rm st}$ (s)	$\tau_{\rm ion}$ (s)	$\dot{N}$ (10^{28} s^{-1})	$Q_{\rm H_2O}$ (kg s^{-1})	$S_{\rm act}$ (m^2)	R (m)	N_e (cm^{-3})
4.98[a]	235^{+9}_{-14}	1020^{+110}_{-150}	$0.59^{+0.06}_{-0.07}$	$58.9^{+6.0}_{-7.0}$	190^{+20}_{-30}	$7.8^{+0.4}_{-0.5}$	$(3.0^{+0.5}_{-0.3}) \times 10^4$
4.98[b]	505^{+20}_{-24}	1900^{+210}_{-250}	0.29 ± 0.03	28.5 ± 2.7	93^{+11}_{-20}	$5.4^{+0.2}_{-0.5}$	$(1.6 \pm 0.2) \times 10^4$
3.60	292^{+12}_{-24}	430^{+50}_{-30}	$8.2^{+0.8}_{-0.9}$	820^{+80}_{-90}	1300^{+130}_{-140}	$20.3^{+1.2}_{-0.8}$	$(7.2^{+0.5}_{-0.7}) \times 10^4$

[a] Main fragment.
[b] Subfragment.

UVCS observations is in our case $\Delta t = (t_{\rm ent} - t_{\rm ej} + n_{\rm exp} t_{\rm exp}) \sim 0.985$ days (where $n_{\rm exp}$ is the exposure number), much greater than the τ_s-values ($\tau_s \sim 10^3$ s) computed by Kimura et al. (2002) around 5 $R_\odot$: as a consequence, the grains have completely sublimated. Tachibana et al. (2002) showed that enstatite ($Mg_2Si_2O_6$, an endmember of pyroxene) evaporates preferentially by the emission of SiO_2, yielding to the formation of a forsterite (Mg_2SiO_4, an endmember of olivine) layer on the surface of enstatite. Hence (see also Kimura et al. 2002), we assumed that the mass loss of pyroxene grains in the sublimation process occurs by the ejection of SiO_2 molecules alone. The authors also showed that, during the SiO_2 evaporation from enstatite, the thickness of the forsterite layer increases with time in the early stage of evaporation and later remains constant at ~4–6 μm, depending on the external temperature. This means that, if we define the equivalent grain radius $R_d = r_m n^{1/3} = 200$ nm $\ll$ 4–6 μm (taking a monomer radius $r_m = 100$ nm and a number $n = 8$ for the monomers of the grain; see Kimura et al. 2002), all the available SiO_2 mass in the grain evaporates.

After the SiO_2 molecules were ejected from the grain, they were photodissociated by the solar radiation. In the literature, there is no estimate for the SiO_2 photodissociation rate: this molecule is likely to behave like CO_2, which has a photodissociation time of ≃113 s at 5 $R_\odot$ (Huebner et al. 1992). Hence, we assume that each SiO_2 molecule photodissociates immediately after evaporation from the pyroxene grains; we assume also that this process produces three neutral atoms.

The neutral O and Si atoms may ionize and/or undergo a charge transfer process, depending on the ambient plasma conditions. At a plasma temperature of $T \simeq 7.2 \times 10^5$ K (see Table 3), the coefficients for the first collisional ionization (including autoionization) for Si and O atoms, respectively, are 1.76×10^{-7} and 5.90×10^{-8} cm^3 s^{-1} (Arnaud & Rothenflug [1985], with revisions described in Verner & Yakovlev [1990]). This means that at the electron density estimated in tail 1 ($N_e = 3.0 \times 10^4$ cm^{-3}), the mean times for the first ionization, respectively, are 186 and 557 s. On the other hand, the charge transfer times for Si and O, respectively, are 121 and 243 s (from the cross sections for the processes; see below). Because the collisional and charge transfer times for Si atoms turn out to be of the same order, we assume that about half the neutral Si atoms undergo charge transfer. We also assume that Si and O atoms undergo no other charge transfer processes after the first one.

From the previous hypotheses, we have that the number densities N(Si) and N(O) of Si and O atoms, respectively, available for charge exchange traveling with the comet are

$$N({\rm Si}) = \frac{1}{2} N_d \frac{m_d({\rm SiO_2})}{m({\rm SiO_2})} \ {\rm cm^{-3}},$$

$$N({\rm O}) = 2 N_d \frac{m_d({\rm SiO_2})}{m({\rm SiO_2})} = 4 N({\rm Si}) \ {\rm cm^{-3}}, \quad (5)$$

where N_d is the unknown dust grain number density, $m_d(SiO_2)$ is the SiO_2 mass of the grain, and $m(SiO_2) = 9.98 \times 10^{-23}$ g is the mass of one SiO_2 molecule. The $m_d(SiO_2)$ is easily computed as

$$m_d({\rm SiO_2}) = \frac{4}{3} \pi f \rho_d R_d^3 = 6.42 \times 10^{-14} \ {\rm g}, \quad (6)$$

where $f \simeq 0.580$ is the pyroxene SiO_2 mass fraction (assuming that the crystal composition formula is $Mg_{1.8}Fe_{0.2}Si_2O_6$; see, e.g., Wooden et al. 1999) and $\rho_d = 3.3$ g cm^{-3} is the bulk grain density (see Kimura et al. 2002). If $\sigma_{\rm cx}$(Si) and $\sigma_{\rm cx}$(O) are the cross sections for inelastic processes in collisions of H^+ ions with neutral Si and O atoms, the formation rate of H atoms can be expressed as

$$N_{\rm H} = N_p N_d \frac{m_d({\rm SiO_2})}{m({\rm SiO_2})} v_p \times \left[\frac{1}{2} \sigma_{\rm cx}({\rm Si}) + 2 \sigma_{\rm cx}({\rm O}) \right] \ {\rm cm^{-3}\ s^{-1}}, \quad (7)$$

where $N_p = N_e$ is the coronal proton density and $v_p = v_r + v_{\rm out} \simeq 420$ km s^{-1} is the proton velocity with respect to the colliding neutrals that move in first approximation with the comet. Equating the number of H atoms formed in a time equal to their lifetime $\tau_{\rm ion}$ to the $\bar{N}_{\rm H}$-value responsible for the constant Lyα background computed above, we have

$$N_d = \bar{N}_{\rm H} \times \left\{ N_p \frac{m_d({\rm SiO_2})}{m({\rm SiO_2})} v_p \left[\frac{1}{2} \sigma_{\rm cx}({\rm Si}) + 2 \sigma_{\rm cx}({\rm O}) \right] \tau_{\rm ion} \right\}^{-1} \ {\rm cm^{-3}}. \quad (8)$$

The cross sections $\sigma_{\rm cx}$(Si) and $\sigma_{\rm cx}$(O) were measured by Kimura et al. (1997). In this work, the authors studied the following charge transfer ionization processes:

$$H^+ + O(^1D) \longrightarrow H + O^+(^2D) - 1.38 \ {\rm eV},$$
$$H^+ + Si(^1D) \longrightarrow H + Si^+(^3D) - 0.628 \ {\rm eV},$$

which involve protons with energy below 1 keV colliding over Si and O atoms. In our case, with the outflow velocity given in § 4 and the cometary radial velocity given in Table 1, the coronal protons collided over neutral atoms with an energy of ~910 eV. With this energy, the charge transfer cross sections given by Kimura et al. (1997) are $\sigma_{\rm cx}({\rm O}) \simeq 2.0 \times 10^{-15}$ cm^2 and $\sigma_{\rm cx}({\rm Si}) \simeq 4.0 \times 10^{-15}$ cm^2.

Using equation (8), we obtain a number density for the pyroxene dust grains of $N_d = 6.2 \times 10^{-10}$ cm^{-3}, which corresponds to a mass density of 6.8×10^{-23} g m^{-3}. In the literature there are no dust measurements for sungrazing comets; the only estimate that we found refers to the grain number density derived from *Vega 1*, *Vega 2*, and *Giotto* spacecraft measurements during the comet P/Halley flyby: at a reference distance of 1000 km from the nucleus, when the comet was at a heliocentric distance between ≃0.8 and 0.9 AU, it turns out that the grains with a mass of $\sim 10^{-14}$ g have a number density of $\sim (1\text{–}2) \times 10^{-5}$ cm^{-3} (Vaisberg et al. 1986; Mazets et al. 1987; McDonnell et al. 1987), hence, ~4 orders of magnitude greater than those in our case. If the grain number density N_d decreases as $\propto 1/d^2$ (where d is the distance from the cometary nucleus), then in the Halley coma $N_d = 6.2 \times 10^{-10}$ cm^{-3} at a distance $d \simeq 1.3 \times 10^5$ km from the nucleus, which corresponds to about 175″ in our observations (Fig. 4).

4.3. *Model Results at* 3.60 $R_\odot$

At 3.60 $R_\odot$, the procedure described in § 4 gives the results shown in Figure 8 and in Table 4; from $t_{\rm st}$ we evaluated the $t_{\rm ent}$-value given in Table 1. At this heliocentric distance we observe only one tail, implying that the secondary fragment disappeared by sublimation along its path between 4.98 and 3.60 $R_\odot$. This can be verified as follows: the thickness of the sublimated layer $R_{\rm subl}$ may be estimated (following Iseli et al. 2002) by

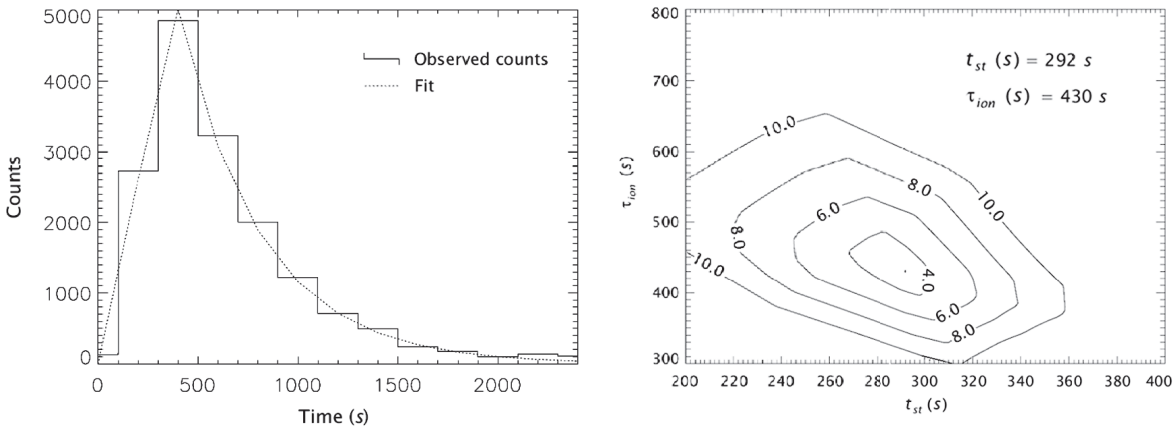

FIG. 8.—*Left*, Observed (*solid line*) and modeled (*dotted line*) Lyα counts at 3.60 $R_\odot$; *right*, iso-χ^2 curves, showing the pair of values for ($\tau_{\rm ion}$, $t_{\rm st}$) at which the χ^2-value is a minimum. Errors in the parameters are determined from the iso-χ^2 curves.

integrating over the cometary orbit the rate of change in radius dR/dt, which is given by

$$\frac{dR}{dt} = \frac{dR}{dr}\frac{dr}{dt} = -0.85\frac{F_\odot(r)(1-A)}{16\pi\rho_{\rm com}L} \text{ cm s}^{-1}, \qquad (9)$$

where r is the heliocentric distance, $F_\odot(r)$ and A are given in § 4, $\rho_{\rm com} \sim 0.6$ g cm^{-3} is the density of porous ice, $L \sim 2.5 \times 10^{10}$ ergs g^{-1} is the latent heat of sublimation of ice, and 0.85 is the fraction of the solar radiation energy that, according to model computations with sungrazers at small heliocentric distances (Iseli et al. 2002), goes into sublimation. Integrating this equation between the two cometary heliocentric distances of 4.98 and 3.60 $R_\odot$ (see Table 1) and taking for $dr/dt \equiv v_r$ the average value $v_r \simeq 2.6 \times 10^7$ cm s^{-1} (Table 1), we obtained the value $R_{\rm subl} \simeq 2.0$ m, which is of the same order as that of the subfragment's estimated radius (Table 4). This means that at this heliocentric distance we cannot see two tails because the subfragment sublimates between 4.98 and 3.60 $R_\odot$.

We note that from the $\dot{N}$-value in Table 4 we derive a radius of 20.3 m, larger than the main-fragment radius at 4.98 $R_\odot$. This is a consequence of the increasing surface $S_{\rm act}$ (see, e.g., Uzzo et al. 2001): at this heliocentric distance, the main nucleus is fragmented into many undetectably small pieces, increasing the surface $S_{\rm act}$ exposed to the solar flux (hence, the derived $\dot{N}$-value) and giving an unrealistic value for the object radius. This explains also why we did not observe the comet at 2.20 $R_\odot$: the comet never reached this heliocentric distance. This scenario is confirmed by the following considerations: if the tensile strength of the cometary nuclear surface is negligible, in a highly idealized case a lower estimate for the heliocentric distance at which the comet would break up is given by the Roche limit $L_{\rm R}$,

$$L_{\rm R} = 2.44\left(\frac{\rho_\odot}{\rho_{\rm com}}\right)^{1/3} R_\odot,$$

where $\rho_\odot = 1.41$ g cm^{-3} is the average solar density; with the density of porous ice given above, this formula yields $L_{\rm R} = 3.24\ R_\odot$. Nongravitational stresses, however, may fracture the comet above $L_{\rm R}$: following Chyba et al. (1993), the fragmentation of the nucleus becomes most probable when the average pressure on the Sunward side is about equal to its tensile strength ($\sim 10^3$–10^5 dynes cm^{-2}). For typical comet material, this happens around 5 $R_\odot$: we can conclude that between about 3.2 and 5 $R_\odot$ (hence, between the heliocentric distances of our observation), the occurrence of cometary nuclear fragmentation events becomes more probable. Fragmentation processes between these two heliocentric distances increase the erosion rate (as discussed above), leading to the observed complete sublimation of the material of the nucleus before 2.20 $R_\odot$; the coexistence of both fragmentation and erosion processes is needed to explain the cometary disappearance above this heliocentric distance.

The derived N_e-value is about half the streamer density given, for instance, by Gibson et al. (1999) or by Strachan et al. (2002) at our heliocentric distances. However, this low N_e-value is realistic because the coronal feature crossed by the comet is very tenuous, nearly unobservable in the LASCO C3 and C2 images (see Fig. 1). An alternative explanation could be that a low N_e-value (i.e., a large value of $\tau_{\rm ion}$) implies a continued production of neutrals after the comet nucleus has passed: this could be material evaporated from dust in the tail (as we supposed at 4.98 $R_\odot$), or it could be small fragments of the comet nucleus, too small to be individually detected; however, on the basis of only our data, it is impossible to distinguish between these explanations.

5. SUMMARY

In conclusion, in this work we report on UVCS observations of a sungrazing comet fragmentation: this was directly observed for the first time by UVCS at 4.98 $R_\odot$ and inferred at 3.60 $R_\odot$. The data at 4.98 $R_\odot$ allow us to observe two tails, which we identify with two fragments for which we estimate the outgassing rates and the radii. The smaller fragment radius is compatible with its total sublimation between 4.98 and 3.60 $R_\odot$, at which only one tail is observed. The observed increase in the $S_{\rm act}$-value at 3.60 $R_\odot$ indicates that the main nucleus fragments into many small pieces between these two heliocentric distances. The slow decrease of the Lyα intensity with time at 4.98 $R_\odot$ was reproduced if we assume a considerable contribution to the neutral H atoms created by the interaction between coronal protons and cometary pyroxene dust grains. This assumption allows us to give for the first time an order-of-magnitude estimate for the pyroxene dust grain number density in sungrazing comets.

Estimates of the kinetic temperature and the electron density of an equatorial coronal hole at 4.98 $R_\odot$ and a coronal streamer at 3.60 $R_\odot$ are consistent with values given in the literature for these parameters near the last solar maximum.

The authors thank the referee, Z. Sekanina, for extremely useful comments that helped improve the manuscript. The authors also wish to thank S. Cranmer and G. Tozzi for useful discussions. This work was supported by NASA grant NAG5-12814. *SOHO* is a mission of international cooperation between ESA and NASA.

REFERENCES

Arnaud, M., & Rothenflug, R. 1985, A&AS, 60, 425
Biesecker, D. A., Lamy, P., St. Cyr, O. C., Llebaria, A., & Howard, R. A. 2002, Icarus, 157, 323
Bion, N. 1751, L'Usage des Globes Celestes et Terrestres (6th ed; Paris: Gúerin)
Brueckner, G. E., et al. 1995, Sol. Phys., 162, 357
Chyba, C. F., Thomas, P. J., & Zahnle, K. J. 1993, Nature, 361, 40
Cooper, E. 1843, Astron. Nachr., 20, 291
Cranmer, S. R., et al. 1999, ApJ, 511, 481
Frazin, R. A., Cranmer, S. R., & Kohl, J. L. 2003, ApJ, 597, 1145
Gibson, S. E., Fludra, A., Bagenal, F., Biesecker, D., Del Zanna, G., & Bromage, B. 1999, J. Geophys. Res., 104, 9691
Henderson, T. 1843, Astron. Nachr., 20, 333
Huebner, W. F., Keady, J. J., & Lyon, S. P. 1992, Ap&SS, 195, 291
Iseli, M., Küppers, M., Benz, W., & Bochsler, P. 2002, Icarus, 155, 350
Kimura, M., Gu, J. P., & Buenker, R. J. 1997, Phys. Rev. A, 55, 2778
Kimura, H., Mann, I., Biesecker, D. A., & Jessberg, E. K. 2002, Icarus, 159, 529
Kirkwood, D. 1880, Observatory, 3, 590
Kohl, J. L., et al. 1995, Sol. Phys., 162, 313
———. 1997, Sol. Phys., 175, 613
Kreutz, H. 1888, Publ. Sternw. Kiel, No. 3
Lindsay, B. G., Sieglaff, D. R., Shafer, D. A., Hakes, C. L., Smith, K. A., & Stebbings, R. F. 1996, Phys. Rev. A, 53, 212
Marocchi, D., Antonucci, E., & Giordano, S. 2001, Ann. Geophys., 19, 135
Marsden, B. G. 1967, AJ, 72, 1170
———. 1989, AJ, 98, 2306
Mazets, E. P., et al. 1987, A&A, 187, 699
McClure, G. W. 1966, Phys. Rev., 148, 47
McDonnell, J. A. M., et al. 1987, A&A, 187, 719
Poletto, G., Suess, S. T., Biesecker, D. A., Esser, R., Gloeckler, G., Ko, Y.-K., & Zurbuchen, T. H. 2002, J. Geophys. Res., 107(A10), 1300
Povich, M. S., et al. 2003, Science, 302, 1949
Raymond, J. C., et al. 1997, Sol. Phys., 175, 645
———. 1998, ApJ, 508, 410
Scholz, T. T., & Walters, H. R. J. 1991, ApJ, 380, 302
Sekanina, Z. 2000, ApJ, 545, L69
———. 2002, ApJ, 576, 1085
———. 2003, ApJ, 597, 1237
Sekanina, Z., & Chodas, P. W. 2004, ApJ, 607, 620
Strachan, L., Suleiman, R., Panasyuk, A. V., Biesecker, D. A., & Kohl, J. L. 2002, ApJ, 571, 1008
Tachibana, S., Tsuchiyama, A., & Nagahara, H. 2002, Geochim. Cosmochim. Acta, 66, 713
Uzzo, M., Raymond, J. C., Biesecker, D. A., Marsden, B., Wood, C., Ko, Y.-K., & Wu, R. 2001, ApJ, 558, 403
Vaisberg, O., Smirnov, V., & Omelchenko, A. 1986, in Proc. 20th ESLAB Symp. on the Exploration of Halley's Comet, Vol. 2: Dust and Nucleus, ed. B. Battrick, E. J. Rolfe, & R. Reinhard (ESA SP-250; Noordwijk: ESA), 17
Verner, D. A., & Yakovlev, D. G. 1990, Ap&SS, 165, 27
Wooden, D. H., Harker, D. E., Woodward, C. E., Butner, H. M., Koike, C., Witteborn, F. C., & McMurtry, C. W. 1999, ApJ, 517, 1034